A linear least squares approach for evaluation of crack tip stress field parameters using DIC.

Harilal R, C. P. Vyasarayani, Ramji M*

Engineering Optics Lab, Department of Mechanical and Aerospace Engineering, IIT Hyderabad, India

Abstract

In the present work, an experimental study is carried out to estimate the mixed-mode stress intensity factors (SIF) for different cracked specimen configurations using digital image correlation (DIC) technique. For the estimation of mixed-mode SIFs using DIC, a new algorithm is proposed for the extraction of crack tip location and coefficients in the multi parameter displacement field equations. From those estimated coefficients, SIF could be extracted. The required displacement data surrounding the crack tip has been obtained using 2D-DIC technique. An open source 2D DIC software Ncorr is used for the displacement field extraction. The presented methodology has been used to extract mixed-mode SIF's for specimen configurations like single edge notch (SEN) specimen and center slant crack (CSC) specimens made out of Al 2014-T6 alloy. The experimental results have been compared with the analytical values and they are found to be in good agreement, thereby confirming the accuracy of the algorithm being proposed.

Keywords: Digital image correlation, Ncorr, Stress Intensity Factor.

1. Introduction

Understanding the failure mechanism in structural components subjected to loading is very important for design engineers. It is a well known fact that the presence of flaws such as cracks and sharp notches in the structural components reduce their strength and leads to initiation of fracture and loss of service life. These cracks arise during manufacturing or because of the induced stresses during thermo-mechanical processing such as welding, heat treatment or during service (due to fatigue and/or creep, stress corrosion, thermal loads etc). The presence of the crack results in the redistribution of stresses and strains around the crack-tip. In fracture mechanics, stress intensity factor (SIF) is used to characterize the stress field around the crack tip. The value of SIF will tell whether the crack will propagate or not under service load. SIF depends on the far field stress (σ), flaw size (a),

*Corresponding author: M. Ramji, Department of Mechanical and Aerospace Engineering, Indian Institute of Technology Hyderabad, ODF Campus, Yeddumailaram 502205, India.

Email address: ramji_mano@iith.ac.in (Ramji M)

component geometry and mode of loading. SIF can be evaluated analytically, numerically and experimentally[1]. Analytical solutions are available for finding SIF for various simple specimen geometries and loading configurations [2]. For complex configurations, SIF need to be extracted either by experiment or by numerical analysis. Numerical methods like finite element method (FEM) requires precise knowledge about the boundary conditions.

The experimental methods are particularly well suited for determining SIF for actual geometry and loading conditions. Also, the techniques of experimental stress analysis can be used to verify the solutions obtained using the other methods. Many researchers have developed and applied methodologies for estimating SIF's involving different experimental techniques. They include whole field non-contact optical methods such as holographic interferometry [3], electronic-speckle-pattern interferometry (ESPI) [4], Moiré interferometry [4, 5], coherent gradient sensing [6], method of caustics [7], photoelasticity [8], digital image correlation [9] etc, as well as contact methods such as measurements using resistance strain gauges [10]. Ramesh *et al.* [11] developed a software based on the multi-paramter stress field equations proposed by Atluri and Kobayashi [12], by implementing the over deterministic least squares technique towards estimation of mixed mode crack tip stress field parameters based on photoelastic data. However, photoelasticity is only suitable for transparent birefringent plastics. Methods like holography and other interferometric techniques are very sensitive to vibration and requires a coherent light source. Interferometric techniques measure the deformation by recording the phase difference of the scattered light wave from the specimen surface before and after deformation. The measurement results are often presented in the form of fringe patterns which requires further processing and phase analysis in order to extract the basic data. Non-interferometric techniques determine the surface deformation by comparing the gray intensity changes of the specimen before and after deformation, and generally have less stringent requirements under actual experimental conditions [13]. Yates *et al.* developed techniques for tracking the crack growth and the evaluation of the mixed mode crack tip stress fields using thermo-elasticity [14]. Recently, Sarangi *et al.* [15] proposed a methodology for accurate estimation of SIF's by optimising the strain gauge locations. They have suggested a new strain gauge based methodology for the experimental determination of the mixed mode SIF's (both K_I and K_{II}). Chu *et al.* developed a computer program based on DIC to estimate displacement components and deformation gradients of an object surface subjected to deformation. Several experiments were performed to demonstrate the viability of this correlation method in experimental mechanics [16].

Amongst these experimental techniques, DIC has become popular for SIF determination because of its relatively simple specimen preparation, ease of use and requirement of less complicated optics. Also it is truly a whole field technique and could be employed for any class of material. It requires specimen surface to be coated with artificial speckle pattern for estimation of displacement and strain fields. It provides information about the displacements and strains by comparing the digital images of the specimen surface coated with artificial speckle pattern in the un-deformed and deformed states respectively. In case of a 2D DIC setup, only one camera is used for the measurement of in-plane surface displacements and strains. Sutton et al. [17] employed 2D-DIC to study the three-dimensional effects near the crack-tip. In order to reduce the experimental noise, they used smoothened u-displacement

and v-displacement field obtained over single edge notch specimen to predict the presence of three-dimensional and/or non-linear zone near the crack-tip. In 2009, Poissant and Barthelat [18] introduced a subset splitting algorithm for the effective application of DIC on discontinuous displacement fields. They proposed a novel approach which enables the subset to split into two sections when a discontinuity is detected. Recently Ronghua Zhu *et al.* [19] investigated the registration accuracies of several subset shapes and control point locations used in DIC technique. They found that the varying the subset shapes affect the registration accuracy while varying the control points have little impact. With the help of these findings, they developed a non-central algorithm for whole field deformation measurement. Jinlong Chen *et al.* [20] presented an improved extended DIC technique to measure discontinuous deformation across the crack. They proposed a non rectangular subset to eliminate the effect of crack width on measurement accuracy. Reng-cai Yang [21] developed a regularized finite-element digital image correlation technique to solve the displacement field with fine and irregular structure. He proposed an algorithm which is capable of resolving displacement field with very fine structure at reasonable accuracy. Ge Yang *et al.* [22] experimentally investigated the damage mechanisms in granites under uniaxial tension. They used DIC for displacement and surface strain measurement. Eskandari *et al.* [23] studied the effect of deformation temperature on the strain localization during tensile loading of micro alloyed steel using an adaptive DIC technique.

However, most of these studies were limited to mode-I crack problems. In 2008, Lopez-Crespo [24] *et al.* developed a generalised approach for determining K_I and K_{II} for a specimen having any mode mixity, directly from displacement fields obtained using DIC for crack growth problem under fatigue loading. The methodologies described in the literature either neglect the error introduced due to ambiguous location of the crack-tip or use non-linear iterative algorithm to locate the crack-tip [25, 26]. Using the whole field displacement data (u_x and u_y) obtained from 2D-DIC, Yoneyama et al. [9, 27] extended the non-linear least square algorithm which considered u_x and u_y displacement components in a combined way. They proposed new convergence criteria based on the correlation coefficient and the sum of absolute values of error between experimentally obtained and theoretically reconstructed displacement fields.

The problem of finding the crack tip stress field parameters and crack tip location can be posed as an optimization problem. The objective function to be minimized is the square of the error between the experimental displacements and curve fitted displacements using multi-parameter displacement field equation. The unknowns to be determined are the parameters in the multi-parameter displacement field equations as well as crack tip location. It is to be noted that the objective function is not quadratic when we consider the crack tip location as an unknown. Using non-linear least square algorithm to minimize the objective function one often finds the local minimum leading to a bad curve fit to the experimental data. In this work, we convert the non-linear least square problem into a sequence of linear least square problems. Therefore, we obtain the global minimum of the objective function.

A 2D-DIC technique is employed to get the whole field displacements over the cracked specimens surrounding the crack tip. The cracked specimen is under tensile loading. An open source 2D DIC software Ncorr is used for displacement extraction. From the whole

field displacement data, SIFs are estimated by solving multi parameter displacement field equations. The proposed method also predicts the position of crack tip with respect to the image coordinate system. Along with the crack tip coordinates, rigid body translations and rotations are also determined. We have studied different specimen configurations like single edge notch specimen (SEN) and center slant crack (CSC) made of 2014-T6 aluminium panel.

2. Test procedure and Specimen fabrication

The cracked panels are made of Al 2014-T6 aluminium alloy plate with a dimension of 40 x 160 x 3 mm^3. The material properties of Al 2014-T6 alloy is given in Table 1 and is taken from the Ref. [28].

Table 1: Material properties of 2014-T6 aluminium alloy obtained from the Ref. [28]

Yield Strength	Young's Modulus	Poisson's ratio
433.34 MPa	71.16 GPa	0.332

The straight edge crack of 8 mm was introduced into the specimen using an electro-discharge machining (EDM) wire cut machine. For creating a center crack, initially a 2 mm hole was drilled at the center of the specimen. This hole serves as the passage for the metallic wire of the EDM machine, which was then used to create a 45 degree inclined crack of length 10 mm at the center. Pre-cracking was done by applying fatigue load in order to generate an initial natural crack with a sharp tip from the notch. During the pre-cracking process, the specimen was monitored closely with a magnifying glass. Liquid dye-penetrant NDT-19 was used to detect any fatigue crack initiation. Using an optical microscope,the lengths of the cracks on both sides of the specimen were measured and the total crack-length was obtained by averaging the two values. The surface of the specimens were then coated with a thin layer of white acrylic paint and sprayed with Carbon black paint using an airbrush to obtain random black-and-white artificial speckle pattern. Figure. 1(a) shows the DIC setup and the loading equipment being used in the present study. The 2D DIC system comprises of a Grasshopper® CCD camera (POINTGREY- GRAS-50S5M-C) of 2448x2048 spatial resolution with a frame rate of 15 fps. A Tamron® zoom lens of 185 mm focal length was mounted on the CCD camera and the camera was connected to a portable computer system with image acquisition card. Light emitting diode (LED) lighting was employed to ensure adequate image contrast. The specimens were loaded using a computer-controlled MTS Landmark® servo-hydraulic cyclic testing machine of 100 kN capacity. Load value for every image being captured was recorded using a separate data acquisition system synchronised with the MTS load cell. In order to estimate the SIF at the crack-tip, the camera was aligned with the test specimens such that the crack faces coincide with horizontal axis of the image co-ordinate system. For SEN specimen, the camera axis was kept horizontal at 0° and for the CSC specimen, the camera axis was kept inclined at 45°. Figure. 1(b) and 1(c) depict the specimen geometry being considered.

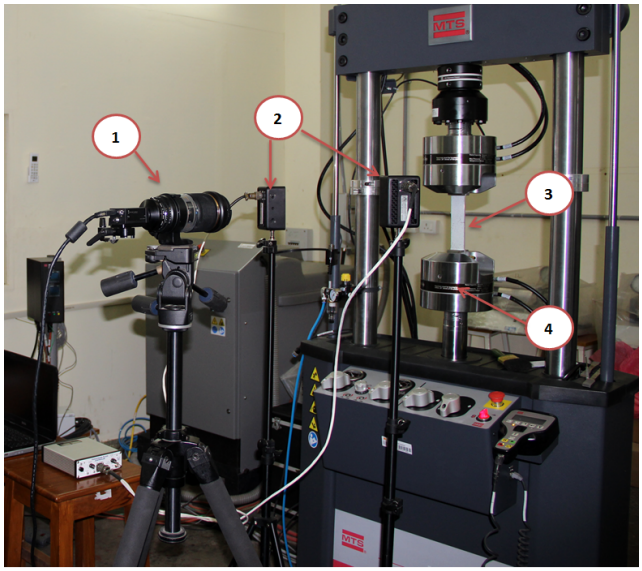

1. Camera at 0° angle
2. Light Sources
3. SEN Specimen
4. Moving Grip

(a)

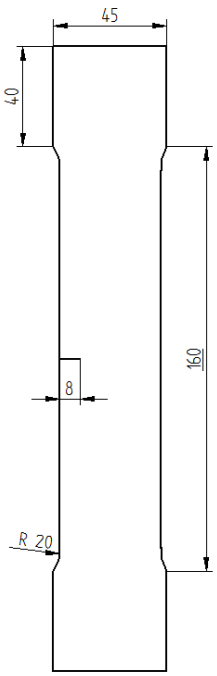

(b)

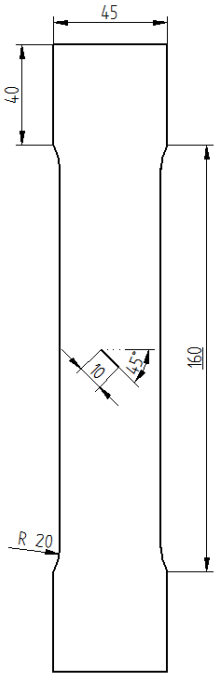

(c)

Figure 1: Experimental setup for SIF estimation involving 2D DIC technique along with specimen geometry (a) Experimental setup (b) SEN specimen dimensions in mm (c) CSC specimen dimensions in mm

3. Experimental estimation of SIF

The images obtained from the camera were processed using an open source, MATLAB® [29] based 2D DIC software Ncorr [30] developed at Georgia Institute of Technology, USA. This software is used for estimating whole field displacement and strain fields. For SIF estimation, an additional SIF estimation module has been developed by the authors for automated data collection and processing. It involves initial calibration window to map physical real world length scale in terms of pixels. The initial crack tip location can be selected using the graphical user interface (GUI). Data is collected from an annular region surrounding the crack-tip, the inner radius of which is chosen more than half of the specimen thickness to avoid the three-dimensional effects at crack tip and also to avoid non-linear zone in the immediate vicinity of the crack tip (Refs. [31, 32]). The region of K dominance is taken at the end of the plastic zone in accordance with the Dugdale [33] and Barenblatt [34] strip yield model. This is a standard practice in linear elastic fracture mechanics (LEFM) based analysis. The outer radius of the annular data collection region is limited such that $r/a \leq 1.5$, where a is the crack length and r is the radius [31] from the crack tip. The inner and outer radii, r_i and r_o of the annular zone for data collection can be specified in the graphical user interface (GUI) as shown in the Fig. 2(a). Here, the pixel data across the

crack faces are omitted during data collection. An Over-deterministic least square algorithm, proposed by Yoneyama et al. [9, 27] is employed in modified form for the estimation of mixed-mode SIFs from the whole field displacement field. The execution of these algorithm is explained in detail in the following sub-sections.

3.1. Multi-parameter displacement field equations

Atluri and Kobayashi [12] represented the two-dimensional displacement field equations for the general mixed mode crack tip displacement field in a concise form as given below:

$$u_x = \sum_{n=1}^{\infty} \frac{A_{In}}{2G} r^{\frac{n}{2}} \{k \cos\frac{n}{2}\theta - \frac{n}{2}\cos(\frac{n}{2}-2)\theta + \{\frac{n}{2} + (-1)^n\}\cos\frac{n}{2}\theta\}$$
$$- \sum_{n=1}^{\infty} \frac{A_{IIn}}{2G} r^{\frac{n}{2}} \{k \sin\frac{n}{2}\theta - \frac{n}{2}\sin(\frac{n}{2}-2)\theta + \{\frac{n}{2} - (-1)^n\}\sin\frac{n}{2}\theta\} \quad (1)$$

$$u_y = \sum_{n=1}^{\infty} \frac{A_{In}}{2G} r^{\frac{n}{2}} \{k \sin\frac{n}{2}\theta + \frac{n}{2}\sin(\frac{n}{2}-2)\theta - \{\frac{n}{2} + (-1)^n\}\sin\frac{n}{2}\theta\}$$
$$- \sum_{n=1}^{\infty} \frac{A_{IIn}}{2G} r^{\frac{n}{2}} \{-k \cos\frac{n}{2}\theta - \frac{n}{2}\cos(\frac{n}{2}-2)\theta + \{\frac{n}{2} - (-1)^n\}\cos\frac{n}{2}\theta\} \quad (2)$$

where u_x and u_y are the displacements along x and y directions respectively, r and θ are the polar coordinates of the data points collected with respect to the crack tip, n is the number of parameters and G is the shear modulus. The parameter $k = (3-\nu)/(1+\nu)$ for plane stress condition, here ν is the Poisson's ratio. The other parameters are defined as $A_{I1} = K_I/\sqrt{2\pi}$, $A_{II1} = K_{II}/\sqrt{2\pi}$ and $A_{I2} = -\frac{\sigma_{0x}}{4}$. The parameter σ_{0x} is the T- stress and is also used for crack tip stress field characterization.

3.2. Solution Procedure

After accounting for rigid body motion, Eq. (1) and Eq. (2) can be recast in the following form

$$u_x = \sum_{n=1}^{\infty} A_{In} f_I(r,\theta) - \sum_{n=1}^{\infty} A_{IIn} f_{II}(r,\theta) + T_x + x(\cos(R)-1) - y\sin(R) \quad (3)$$

$$u_y = \sum_{n=1}^{\infty} A_{In} g_I(r,\theta) - \sum_{n=1}^{\infty} A_{IIn} g_{II}(r,\theta) + T_y + y(\cos(R)-1) + x\sin(R) \quad (4)$$

In the above equations (Eq. (3) and Eq. (4)), T_x and T_y are the rigid body translations in x and y directions and R is the rigid body rotation. The terms f_I, f_{II}, g_I and g_{II} are trigonometric functions in terms of co-ordinates r and θ.

In many cases, it is difficult to find the exact location of the crack-tip due to low spatial resolution of the images being captured. The crack tip location (x_c, y_c) can be treated

as unknown parameters along with the coefficients of Eq. (3) and Eq. (4). The crack tip location is related to r and θ as follows:

$$r = \sqrt{(x - x_c)^2 + (y - y_c)^2} \tag{5}$$

$$\theta = \tan^{-1}\left(\frac{y - y_c}{x - x_c}\right) \tag{6}$$

where, x_c and y_c are the locations of the crack tip relative to an arbitrary cartesian co-ordinate frame whose x and y axes are parallel to that of crack tip co-ordinate system.

For practical computational reasons the number of terms in Eq. (3) and Eq. (4) are truncated to a finite number. For a single point p, the n parameter Eq. (3) and Eq. (4) can be rewritten in matrix form as

$$\underbrace{\begin{Bmatrix} u_{xp} \\ u_{yp} \end{Bmatrix}}_{\boldsymbol{u_p}} = \underbrace{\begin{bmatrix} f_{I1}(r_p,\theta_p) & g_{I1}(r_p,\theta_p) \\ f_{I2}(r_p,\theta_p) & g_{I2}(r_p,\theta_p) \\ \vdots & \vdots \\ f_{In}(r_p,\theta_p) & g_{In}(r_p,\theta_p) \\ -f_{II1}(r_p,\theta_p) & -g_{II1}(r_p,\theta_p) \\ -f_{II2}(r_p,\theta_p) & -g_{II2}(r_p,\theta_p) \\ \vdots & \vdots \\ -f_{IIn}(r_p,\theta_p) & -g_{IIn}(r_p,\theta_p) \\ 1 & 0 \\ 0 & 1 \\ x_p & y_p \\ -y_p & x_p \end{bmatrix}^{\mathrm{T}}}_{\boldsymbol{Q_p}} \underbrace{\begin{Bmatrix} A_{I1} \\ A_{I2} \\ \vdots \\ A_{In} \\ A_{II1} \\ A_{II2} \\ \vdots \\ A_{IIn} \\ T_x \\ T_y \\ \gamma_1 \\ \gamma_2 \end{Bmatrix}}_{\boldsymbol{a}} \tag{7}$$

Here, we introduced barycentric parameters, $\gamma_1 = \cos(R) - 1$ and $\gamma_2 = \sin(R)$. There by allowing us to write Eq. (7) in the following form.

$$\boldsymbol{u_p} = \boldsymbol{Q_p^{\mathrm{T}}}\ \boldsymbol{a} \tag{8}$$

Such an approach is commonly used in parameter identification problems in multibody dynamics [35]. For a set of m collected data points surrounding crack tip, the assembled set of matrices for n parameter solution can be written as

$$\boldsymbol{u} = \mathbf{C}\,(x_c, y_c)\,\boldsymbol{a} \tag{9}$$

where $\boldsymbol{u} = [\boldsymbol{u_1^{\mathrm{T}}}\ \boldsymbol{u_2^{\mathrm{T}}}\ \ldots\ \boldsymbol{u_m^{\mathrm{T}}}]^{\mathrm{T}}$ and $\mathbf{C} = [\boldsymbol{Q_1^{\mathrm{T}}}\ \boldsymbol{Q_2^{\mathrm{T}}}\ \ldots\ \boldsymbol{Q_m^{\mathrm{T}}}]^{\mathrm{T}}$. Here, $\boldsymbol{u}$ is the vector consisting of displacements obtained from the experimental data. $\mathbf{C}$ is a rectangular matrix of the order $2m \times (2n + 4)$ which is dependent on x_c and y_c and $\boldsymbol{a}$ is the vector consisting of

unknown mode I and mode II parameters along with the translation and rotation terms. We will find the values of x_c, y_c and $\boldsymbol{a}$ by minimizing the following objective function:

$$J(x_c, y_c, \boldsymbol{a}) = \frac{1}{2}(\boldsymbol{u} - \mathbf{C}\,(x_c, y_c)\,\boldsymbol{a})^{\mathrm{T}}(\boldsymbol{u} - \mathbf{C}\,(x_c, y_c)\,\boldsymbol{a}) \tag{10}$$

It should be noted that J is not a quadratic function due to its dependency on the unknown crack tip coordinates x_c and y_c. However, for every known x_c and y_c, the objective function becomes quadratic in parameters and the following closed form solution exists for the unknown parameters ($\boldsymbol{a}$) at which the objective function (Eq. (10)) attains a global minimum and is given by:

$$\boldsymbol{a} = (\mathbf{C}^{\mathrm{T}}\mathbf{C})^{-1}\mathbf{C}^{\mathrm{T}}\boldsymbol{u} \tag{11}$$

where $(\mathbf{C}^{\mathrm{T}}\mathbf{C})^{-1}\mathbf{C}^{\mathrm{T}}$ is the pseudo inverse of $\mathbf{C}$.

We select multiple $(x_{ci}, y_{cj}), i = 1, 2, .., p, j = 1, 2, ..., p$ locations around the crack tip as shown in Fig. 2(b) and for each of these location we obtain the unknown parameters $\mathbf{a}_{ij}$ using Eq. (11). For every (x_{ci}, y_{cj}), having known $\mathbf{a}_i$ we calculate J_{ij}. Out of all the grid points (see Fig. 2(b)) we select the crack tip location $(x_c^*, y_c^*) = (x_{ci}, y_{cj})$ and unknown parameters $\mathbf{a}^* = \mathbf{a}_{ij}$ corresponding to the location (x_{ci}, y_{cj}) at which J_{ij} attains the lowest value. Mathematically our idea to find the optimal parameters and crack tip location can be represented as follows:

$$[\boldsymbol{a}^{*\mathrm{T}} \quad x_c^* \quad y_c^*]^{\mathrm{T}} = \arg\min\,[\min\,(J_{ij}, i = 1, 2, ..., p,\ j = 1, 2, ..., p)] \tag{12}$$

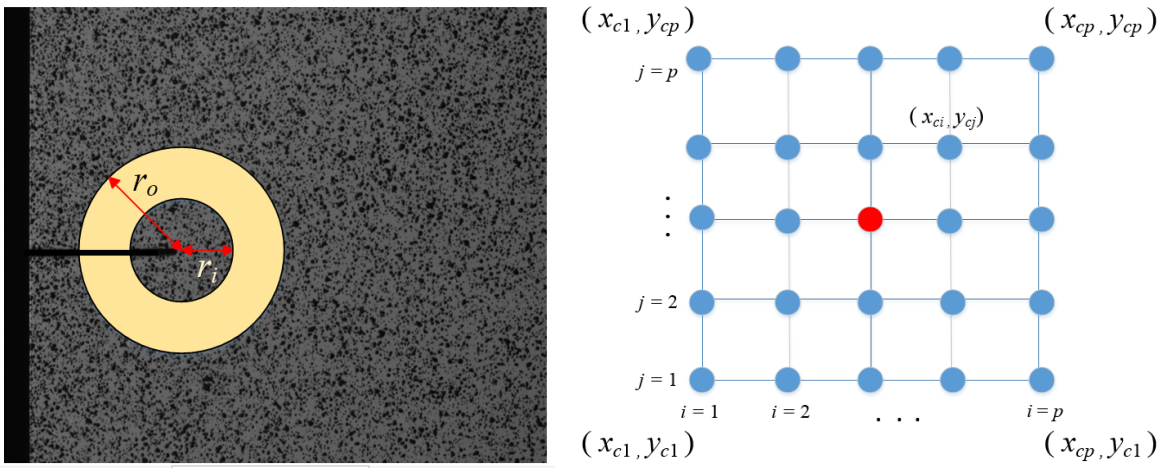

(a) (b)

Figure 2: Data collection zone and corresponding square grid (a) Schematic diagram of the annular region used in data collection for SIF estimation in case of SEN specimen along with the speckle image (b) Schematic representation of the square grid used for obtaining optimal crack tip location

The procedure for obtaining optimal values of $\boldsymbol{a}$ and crack tip coordinates (x_c, y_c) presented in this section can be summarized in the algorithmic form as shown below:

Algorithm 1 Algorithm

Minimise the error $J(x_c, y_c, r, n, \boldsymbol{a})$
for x_c from x_{c1} to x_{cp} **do**
  for y_c from y_{c1} to y_{cp} **do**
    for r from r_i to r_o **do**
      for n from n_s to n_e **do**

$$\boldsymbol{a} = (\mathbf{C}^{\mathrm{T}}\mathbf{C})^{-1}\mathbf{C}^{\mathrm{T}}\boldsymbol{u}$$

$$J(x_c, y_c, \boldsymbol{a}) = \frac{1}{2}(\boldsymbol{u} - \mathbf{C}\,(x_c, y_c)\,\boldsymbol{a})^{\mathrm{T}}(\boldsymbol{u} - \mathbf{C}\,(x_c, y_c)\,\boldsymbol{a})$$

      end for
    end for
  end for
end for

$$[\boldsymbol{a}^{*\mathrm{T}} \quad x_c^* \quad y_c^*]^{\mathrm{T}} = arg\,min\,min\,[J_{ij}, i = 1, 2, ..., p,\ j = 1, 2, ..., p]$$

where x_c and y_c are the crack tip coordinates, x_{c1} and x_{cp} are the minimum and maximum x coordinate values of the square grid as shown in Fig. 2(b), y_{c1} and y_{cp} are the minimum and maximum y coordinate values of the square grid as shown in Fig. 2(b), r_i and r_o are the inner and outer radii of data collection as shown in Fig. 2(a), n_s and n_e are the minimum and maximum number of unknown parameters (see Eq. (7)).

4. Results and Discussions

The displacement data is extracted using an open source 2D DIC software Ncorr which has been found to generate accurate displacement data from input speckle images [36]. The displacement field data for SEN and CSC specimens obtained from Ncorr is used as the input for the SIF estimation algorithm to determine the mixed mode SIFs.

4.1. Experimental determination of SIF for SEN specimen

Using the automated data collection interface incorporated in the SIF estimation software, both u_x and u_y displacement data are collected within an annular region specified around the crack tip along with the corresponding pixel coordinates obtained for SEN specimen being subjected to a tensile load of 8 kN (66.6 MPa). An approximate location of the crack tip is selected using the crack tip selection interface. With the selected crack tip as center, a square with $0.2\,mm$ side length and a grid size of $0.02\,mm$ is created. For each of these grid points, the value of $\boldsymbol{a}$ is computed. The value of $\boldsymbol{a}$ corresponding to the lowest J value is used to compute K_I. Figure. 3 shows the normalized error plot with respect to x and y crack tip coordinates selected from the grid. The red circle along with an arrow shows the zone of least error which corresponds to exact crack tip location.

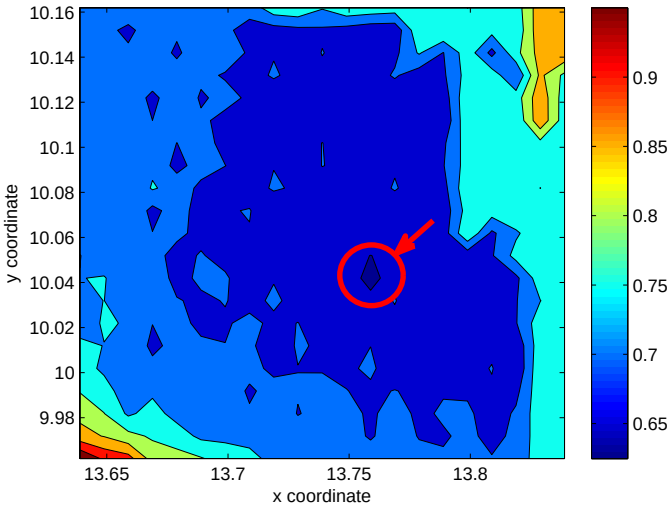

Figure 3: Normalized error plot for experimental estimation of SIFs for SEN specimen

The experimentally estimated K_I determined from the relation $A_{I1} = K_I/\sqrt{2\pi}$ is found to be 449.8741 $MPa\sqrt{mm}$. The analytical expression of the SIF for SEN specimen [2] is as follows

$$K_I = \sigma\sqrt{\pi a}F(\alpha) \tag{13}$$

where σ is the far-field stress and a is the crack length. $F(\alpha)$ can be expanded as

$$F(\alpha) = 1.12 - 0.231\alpha + 10.55\alpha^2 - 21.72\alpha^3 + 30.39\alpha^4$$

where α is crack length to width ratio a/W whose value is 0.2.

Along with the SIF value, the crack tip coordinates, T_x, T_y and R are also estimated. The values of T_x, T_y and R for the 7 parameter solution are found to be -0.03982, 0.1467 and 0.0000457 respectively. The reason for choosing 7 parameters is based on the convergence of K_I value. It is to be noted that the co-ordinates of the crack-tip are with respect to the image co-ordinate system. The coordinates of the location of the crack tip through manual selection are found to be 13.728 mm and 10.061 mm. After the solution search, the crack tip coordinates corresponding to the least error zone is returned. The x and y coordinates of the predicted crack tip coordinates are found to be 13.768 mm and 10.041 mm. The analytical SIF is calculated using Eq. (13) and is found to be 458.0994 $MPa\sqrt{mm}$. The experimentally estimated SIF value is found to be close to the analytical value with an error of 1.8%.

The values of different parameters for 2, 4 and 7 parameter solution for SEN specimen are summarized in Table 2. As an additional check, the reconstructed and experimental (red markers) displacements fields for 7 parameter solution are superposed on each other in case of SEN specimen and is shown in Fig. 4. Here, one could visually reconfirm that the 7 parameter solution aptly predicts the experimental displacement fields.

Table 2: Crack tip fracture parameters for SEN specimen

	2-parameter	4-parameter	7-parameter
K_I (MPa$\sqrt{mm}$)	282.4899	380.8687	449.8741
A_{I1} (MPa$(mm)^{1/2}$)	108.4066	150.8950	175.3587
A_{I2} (MPa)	-13.3757	-22.1636	-29.0510
A_{I3} (MPa$(mm)^{-1/2}$)		7.8054	8.6279
A_{I4} (MPa$(mm)^{-1}$)		-0.5936	0.05096
A_{I5} (MPa$(mm)^{-3/2}$)			-0.6144
A_{I6} (MPa$(mm)^{-2}$)			0.1012
A_{I7} (MPa$(mm)^{-5/2}$)			-0.0148

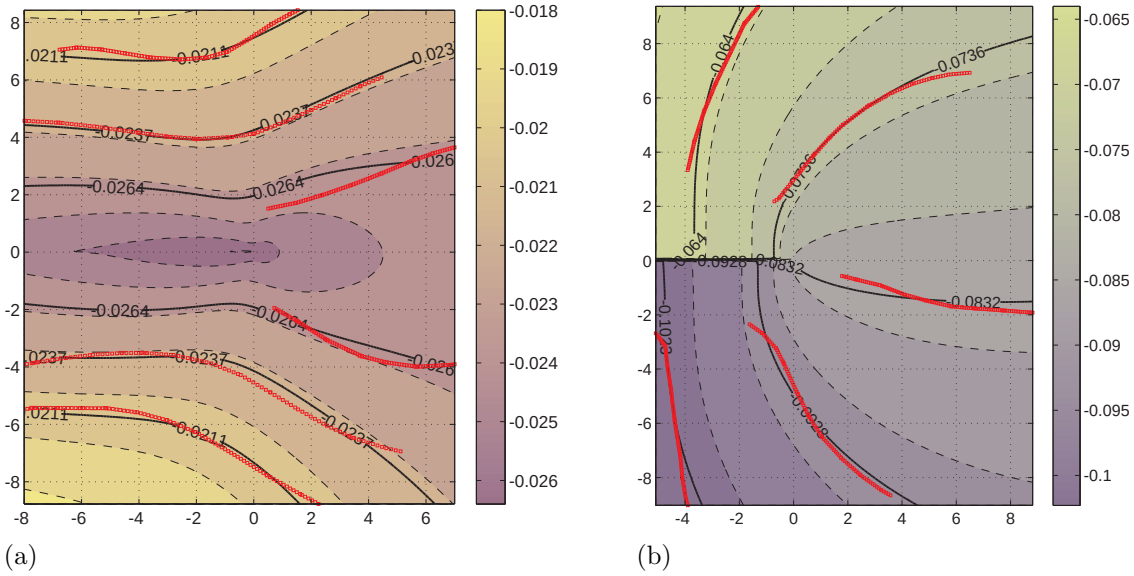

Figure 4: Experimental (red markers) and reconstructed displacements fields obtained for 7 parameter solution superposed over each other in case of SEN specimen (a) u_x displacement field (in mm)(b) u_y displacement field (in mm)

4.2. Experimental determination of SIF for CSC specimen

The same procedure of data collection used for the SIF estimation in the case of SEN specimen as explained in section 4.1 is followed for CSC specimen as well. Fig. 5 shows the normalized error plot with respect to x and y crack tip coordinates selected from the grid for CSC specimen at a tensile load of 4 kN (33.33 MPa). The red circle and arrow shows the zone of least error which corresponds to exact crack tip location. The analytical values

of K_I and K_{II} for the CSC specimen are estimated from the expressions taken from Ref. [2]

$$K_I = \sigma\sqrt{\pi a}F_I(\alpha), \quad K_{II} = \sigma\sqrt{\pi a}F_{II}(\alpha) \tag{14}$$

The F_I and F_{II} values are found to be 0.5181 and 0.5072 for a 45° center inclined crack respectively [2]. The analytical values of K_I and K_{II} for the given loading condition are found to be 68.4467 $MPa\sqrt{mm}$ and 67.0067 $MPa\sqrt{mm}$ respectively [2]. The experimentally estimated K_I and K_{II} values are found to be 62.9468 $MPa\sqrt{mm}$ and 62.5198 $MPa\sqrt{mm}$ respectively. Here too, the 7 parameter solution is found to be accurate as the reconstructed displacement field coincides accurately with the experimental data (See Fig. 6). The percentage deviation in experimentally determined K_I and K_{II} values from the analytical values are 8.035%and 6.69% respectively. The values of T_x, T_y and R for the 7 parameter solution is found to be 0.07193, 0.0731 and 0.000568 respectively. The coordinates of the location of the crack tip through manual selection are found to be 12.8314 and 15.7639 (in mm). The x and y coordinates of the predicted location of the crack tip are found to be 12.618 and 15.783 (in mm). The values of various fracture parameters for 2, 4 and 7 parameter solution estimated in case of CSC specimen are summarised in Table 3.

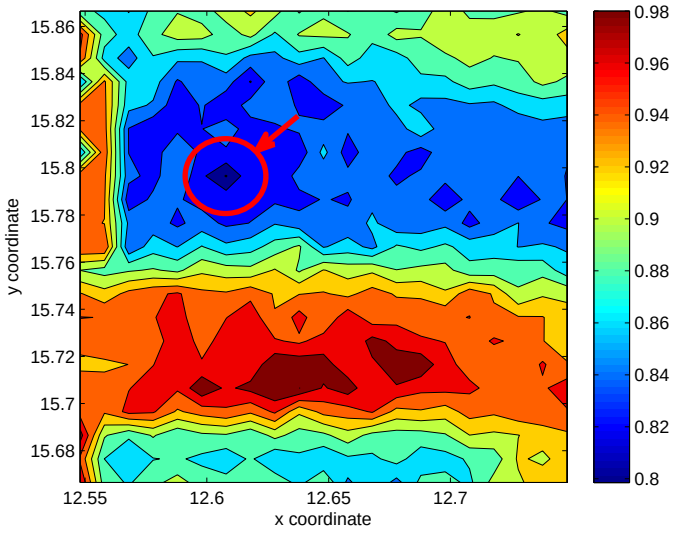

Figure 5: Normalized error plot for experimental estimation of SIFs for CSC specimen

Table 3: Crack tip fracture parameters for CSC specimen

	2-parameter	4-parameter	7-parameter
K_I (MPa$\sqrt{mm}$)	33.9822	94.5614	62.9468
K_{II} (MPa$\sqrt{mm}$)	78.8870	70.8966	62.5198
A_{I1} (MPa$(mm)^{1/2}$)	13.5569	37.7245	25.1121
A_{I2} (MPa)	0.2298	-6.6442	2.1702
A_{I3} (MPa$(mm)^{-1/2}$)		8.4157	5.9959
A_{I4} (MPa$(mm)^{-1}$)		-0.6307	-0.5789
A_{I5} (MPa$(mm)^{-3/2}$)			0.9902
A_{I6} (MPa$(mm)^{-2}$)			-0.1906
A_{I7} (MPa$(mm)^{-5/2}$)			0.1403
A_{II1} (MPa$(mm)^{1/2}$)	31.4713	28.2836	24.9418
A_{II2} (MPa)	0.0000	0.0000	0.0000
A_{II3} (MPa$(mm)^{-1/2}$)		4.6796	4.3665
A_{II4} (MPa$(mm)^{-1}$)		-0.5292	-1.3957
A_{II5} (MPa$(mm)^{-3/2}$)			0.6901
A_{II6} (MPa$(mm)^{-2}$)			-0.3779
A_{II7} (MPa$(mm)^{-5/2}$)			0.07116

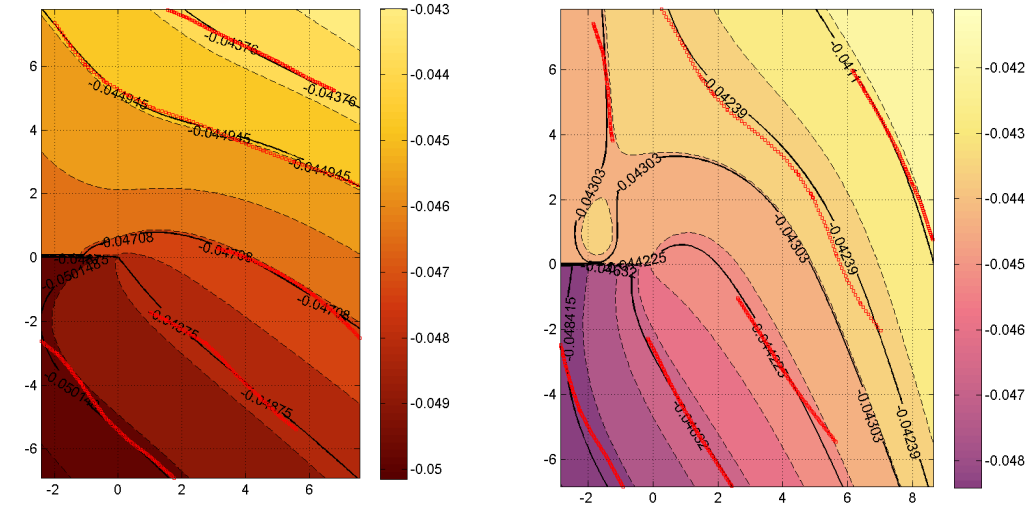

(a) (b)

Figure 6: Experimental (red markers) and reconstructed displacements fields obtained for 7 parameter solution superposed over each other in case of CSC specimen (a) u_x displacement field (in mm)(b) u_y displacement field (in mm)

The SIF values for SEN and CSC specimens determined above are obtained using 7 parameters in the series solution for u_x and u_y in the multi-parameter displacement field equation (see Eq. (1) and Eq. (2)). In order to decide upon the number of parameters required for the accurate estimate, a convergence study has been carried out. It has been found that J (see Eq. (10)) attains a constant value after iteratively increasing the number of parameters to 7 for both SEN and CSC specimens as shown in Fig. 7(a) and Fig. 7(b) respectively.

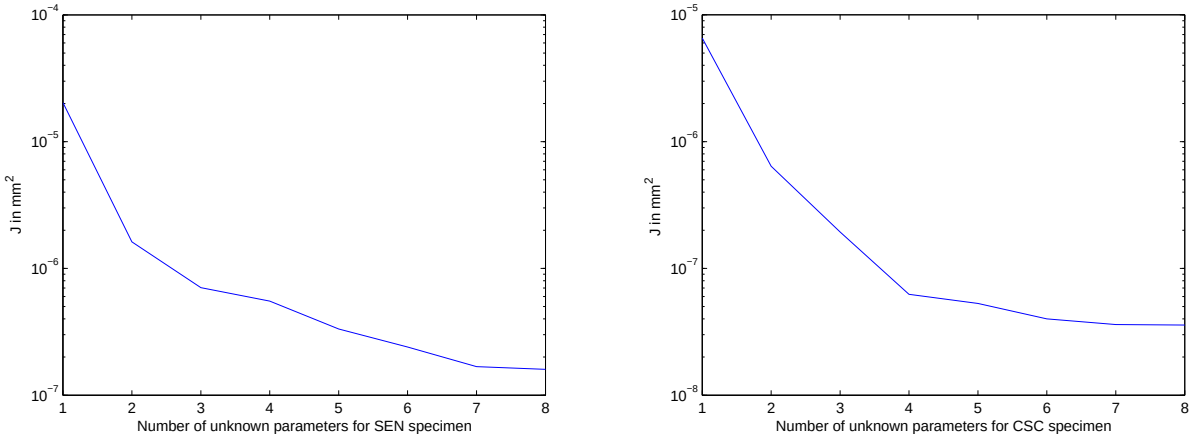

(a) (b)

Figure 7: J variation with increasing number of parameters (a) SEN specimen (b) CSC specimen

With the increase in number of parameters, the SIF values converge. With further increase in parameter values after 7, no significant change in SIF value is observed. This is true for both SEN and CSC specimens as shown in Figs. 8(a),8(b) and 8(c).

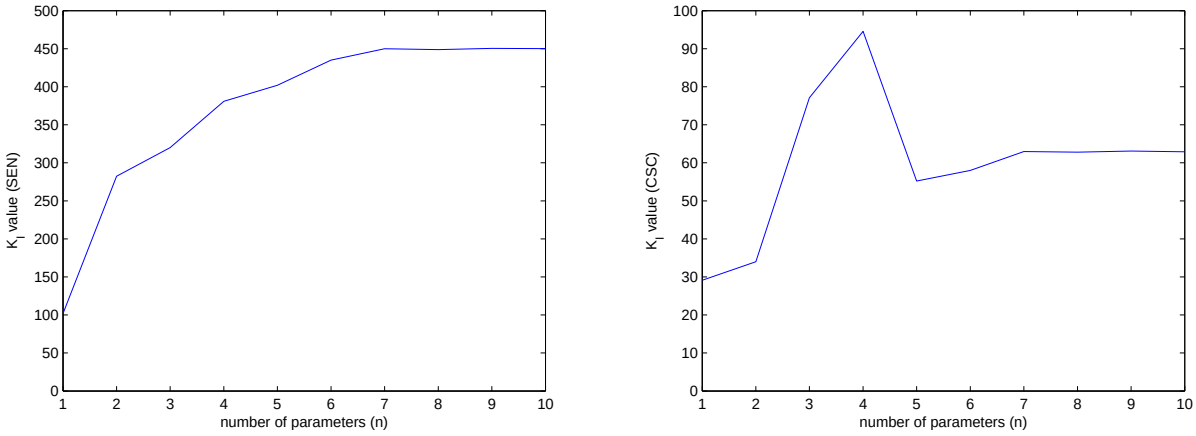

(a) (b)

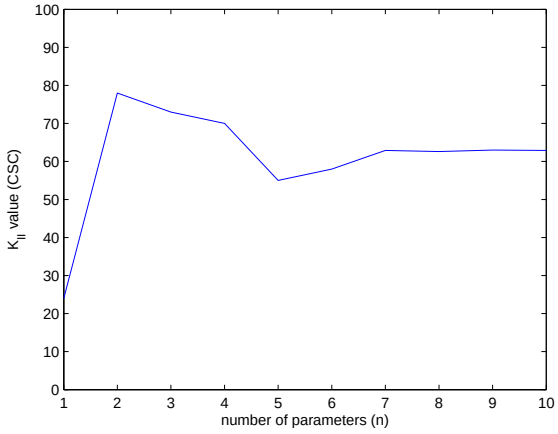

(c)

Figure 8: Variation of mixed mode SIFs for SEN and CSC specimens with n (a) Variation of K_I for SEN specimen (b) Variation of K_I for CSC specimen (c) Variation of K_{II} for CSC specimen

5. Conclusions

In this work, an experimental study is carried out to estimate the fracture parameters in cracked aluminium panels. Here, both SEN and CSC specimen configurations are studied. Full field crack tip displacement field over the surface of the panel is estimated using 2D-DIC technique. An over deterministic linear least square technique is successfully implemented for SIF estimation involving multi-parameter displacement field equation. By introducing the barycentric parameters and by exploiting the fact that crack tip location has to be present in a certain closed domain, the nonlinear parameter identification problem has been converted into a sequence of linear quadratic optimisation problems. This approach is much

faster than the conventional iterative scheme existing in the literature [8, 9]. Apart from SIF extraction, a new optimisation based approach is also integrated for exact crack tip coordinate location. Further, we have included rigid body rotation terms in the study for accurate estimation of SIFs. The estimated SIF values for both the specimen configurations are found to be in close match with the analytical estimates, thereby confirming the accuracy of the developed methodology.

Acknowledgments

We thank Dr. Viswanath of IIT Hyderabad for several interesting discussions during the course of the study.

References

[1] T. L. Anderson, Fracture mechanics: fundamentals and applications, CRC press, 2005.
[2] Y. Murakami, Stress Intensity Factors Handbook, Pergamon Pr, 1987.
[3] T. Dudderar, H. Gorman, The determination of mode i stress-intensity factors by holographic interferometry, Experimental Mechanics 13 (4) (1973) 145–149.
[4] A. Moore, J. Tyrer, Phase-stepped espi and moiré interferometry for measuring stress-intensity factor andj integral, Experimental mechanics 35 (4) (1995) 306–314.
[5] H. Rossmanith, Analysis of crack-tip moiré fringe patterns, International Journal of Fracture 21 (2) (1983) 83–106.
[6] S. Ramaswamy, H. Tippur, L. Xu, Mixed-mode crack-tip deformations studied using a modified flexural specimen and coherent gradient sensing, Experimental mechanics 33 (3) (1993) 218–227.
[7] Y. Kawagishi, M. Shozu, Y. Hirose, Experimental evaluation of stress field around crack tip by caustic method, Mechanics of materials 33 (12) (2001) 741–757.
[8] R. J. Sanford, Determining fracture parameters with full-field optical methods, Experimental Mechanics 29 (3) (1989) 241–247.
[9] S. Yoneyama, Y. Morimoto, M. Takashi, Automatic evaluation of mixed-mode stress intensity factors utilizing digital image correlation, Strain 42 (1) (2006) 21–29.
[10] M. Carboni, Strain-gauge compliance measurements near the crack tip for crack closure evaluation: Applicability and accuracy, Engineering fracture mechanics 74 (4) (2007) 563–577.
[11] K. Ramesh, S. Gupta, A. A. Kelkar, Evaluation of stress field parameters in fracture mechanics by photoelasticityrevisited, Engineering Fracture Mechanics 56 (1) (1997) 25–45.
[12] A. K. S.N. Atluri, Mechanical responses of materials, A.S. Kobayashi (Ed.), Handbook on Experimental Mechanics, John Wiley & Sons, New York, 1993.
[13] B. Pan, K. Qian, H. Xie, A. Asundi, Two-dimensional digital image correlation for in-plane displacement and strain measurement: a review, Measurement science and technology 20 (6) (2009) 062001.
[14] J. Yates, M. Zanganeh, R. Tomlinson, M. Brown, F. D. Garrido, Crack paths under mixed mode loading, Engineering Fracture Mechanics 75 (3) (2008) 319–330.
[15] H. Sarangi, K. Murthy, D. Chakraborty, Optimum strain gage locations for accurate determination of the mixed mode stress intensity factors, Engineering Fracture Mechanics 88 (2012) 63–78.
[16] T. Chu, W. Ranson, M. Sutton, Applications of digital-image-correlation techniques to experimental mechanics, Experimental mechanics 25 (3) (1985) 232–244.
[17] M. Sutton, J. Turner, Y. Chao, H. Bruck, T. Chae, Experimental investigations of three-dimensional effects near a crack tip using computer vision, International journal of fracture 53 (3) (1992) 201–228.
[18] J. Poissant, F. Barthelat, A novel subset splitting procedure for digital image correlation on discontinuous displacement fields, Experimental mechanics 50 (3) (2010) 353–364.

[19] R. Zhu, H. Xie, Z. Hu, L. Jiang, B. Guo, C. Li, Performances of different subset shapes and control points in subset-based digital image correlation and their applications in boundary deformation measurement, Applied optics 54 (6) (2015) 1290–1301.
[20] J. Chen, N. Zhan, X. Zhang, J. Wang, Improved extended digital image correlation for crack tip deformation measurement, Optics and Lasers in Engineering 65 (2015) 103–109.
[21] R.-c. Yang, A regularized finite-element digital image correlation for irregular displacement field, Optics and Lasers in Engineering 56 (2014) 67–73.
[22] G. Yang, Z. Cai, X. Zhang, D. Fu, An experimental investigation on the damage of granite under uniaxial tension by using a digital image correlation method, Optics and Lasers in Engineering 73 (2015) 46–52.
[23] M. Eskandari, M. Yadegari-Dehnavi, A. Zarei-Hanzaki, M. Mohtadi-Bonab, R. Basu, J. Szpunar, In-situ strain localization analysis in low density transformation-twinning induced plasticity steel using digital image correlation, Optics and Lasers in Engineering 67 (2015) 1–16.
[24] P. Lopez-Crespo, A. Shterenlikht, E. Patterson, J. Yates, P. Withers, The stress intensity of mixed mode cracks determined by digital image correlation, The Journal of Strain Analysis for Engineering Design 43 (8) (2008) 769–780.
[25] P. Luo, Y. Chao, M. Sutton, W. Peters III, Accurate measurement of three-dimensional deformations in deformable and rigid bodies using computer vision, Experimental Mechanics 33 (2) (1993) 123–132.
[26] G. Han, M. Sutton, Y. Chao, A study of stationary crack-tip deformation fields in thin sheets by computer vision, Experimental Mechanics 34 (2) (1994) 125–140.
[27] S. Yoneyama, T. Ogawa, Y. Kobayashi, Evaluating mixed-mode stress intensity factors from full-field displacement fields obtained by optical methods, Engineering fracture mechanics 74 (9) (2007) 1399–1412.
[28] K. Naresh Reddy, M. Ramji, Material characterisation of al-2014 t6 alloy using 3d-digital image correlation technique, Proceedings of International conference on metallurgical and materials Processes, products and applications.
[29] MATLAB, version 8.0 (R2012b), The MathWorks Inc., Natick, Massachusetts, 2012.
[30] Ncorr 2d-dic software, `http://www.ncorr.com`.
[31] G. P. Mogadpalli, V. Parameswaran, Determination of stress intensity factor for cracks in orthotropic composite materials using digital image correlation, Strain 44 (6) (2008) 446–452.
[32] A. Shukla, B. Agarwal, B. Bhushan, Determination of stress intensity factor in orthotropic composite materials using strain gages, Engineering fracture mechanics 32 (3) (1989) 469–477.
[33] D. Dugdale, Yielding of steel sheets containing slits, Journal of the Mechanics and Physics of Solids 8 (2) (1960) 100–104.
[34] G. I. Barenblatt, The mathematical theory of equilibrium cracks in brittle fracture, Advances in applied mechanics 7 (1) (1962) 55–129.
[35] C. P. Vyasarayani, T. Uchida, J. McPhee, Nonlinear parameter identification in multibody systems using homotopy continuation, Journal of Computational and Nonlinear Dynamics 7 (1) (2012) 011012.
[36] H. Ramesh, M. Ramji, Adaptation of open source 2d dic software ncorr for solid mechanics applications, in: 9th International Symposium on Advanced Science and Technology in Experimental Mechanics, 2014.